FISEVIER

Contents lists available at ScienceDirect

# Journal of Non-Crystalline Solids: X

journal homepage: www.sciencedirect.com/journal/journal-of-non-crystalline-solids-x





# Structure factor of a phase separating binary mixture with natural and forceful interconversion of species

Thomas J. Longo <sup>a,\*</sup>, Nikolay A. Shumovskyi <sup>b</sup>, Salim M. Asadov <sup>a,c</sup>, Sergey V. Buldryev <sup>b,d</sup>, Mikhail A. Anisimov <sup>a,e</sup>

- <sup>a</sup> Institute for Physical Science and Technology, University of Maryland, College Park, MD 20742, USA
- <sup>b</sup> Department of Physics, Boston University, Boston, MA 02215, USA
- <sup>c</sup> Institute of Catalysis and Inorganic Chemistry, Azerbaijan National Academy of Sciences, Baku AZ1143, Azerbaijan
- <sup>d</sup> Department of Physics, Yeshiva University, New York, NY 10033, USA
- e Department of Chemical and Biomolecular Engineering, University of Maryland, College Park, MD 20742, USA

#### ARTICLE INFO

#### Keywords: Spinodal decomposition Phase separation Structure factor Interconversion of species

#### ABSTRACT

Using a modified Cahn-Hilliard-Cook theory for spinodal decomposition in a binary mixture that exhibits both diffusion and interconversion dynamics, we derive the time-dependent structure factor for concentration fluctuations. We compare the theory and obtain a qualitative agreement with simulations of the temporal evolution of the order parameter and structure factor in a nonequilibrium Ising/lattice-gas hybrid model in the presence of an external source of forceful interconversion. In particular, the characteristic size of the steady-state phase domain is predicted from the lower cut-off wavenumber of the amplification factor in the generalized spinodal-decomposition theory.

#### 1. Introduction

C. Austin Angell's pioneering work published 50 years ago hypothesized that the thermodynamic anomalies of liquid water could be attributed to the existence of two supramolecular states [1]. Later, this idea was further developed to predict liquid-liquid phase separation in supercooled water below the temperature of homogeneous ice formation [2,3], as well as in the vitreous state of various substances [4–9]. This phenomenon, known as "liquid and glassy polyamorphism" [10,11], could be attributed to the interconversion between two alternative molecular or supramolecular states [12]. In this work, we investigate the effects of interconversion between alternative species in a binary mixture on the phase separation and phase domain growth.

Previous studies of a hybrid Ising/lattice-gas model exhibiting both interconversion and diffusion dynamics [13] and a chiral model with interconversion of species [14,15] have demonstrated that interconversion dynamics breaks the symmetry of phase separation. As a result, depending on the rate of interconversion, to circumvent the energetically unfavorable formation of an interface, one stable phase will grow at the expense of the other, a phenomenon known as "phase

amplification" [13,16]. However, if the alternative species are forced to interconvert due to an external source, then the formation of interfaces between species may become more favorable and the system may phase separate into steady-state microphase domains [16]. Previous studies of a phase separating binary-lattice in the presence of an external interconversion force [17–19] and a chiral model with dissipative intermolecular forces [15] have demonstrated steady-state microphase separation.

In this work, we consider a symmetric binary mixture that, when quenched along critical composition below the critical temperature of demixing, will phase separate via spinodal decomposition [20]. Simultaneously, the alternative species may interconvert either naturally or forcefully. To characterize the formation of phase domains, we calculate the temporal evolution of the structure factor for the concentration fluctuations. We describe the time-dependent structure factor through two characteristic wavenumbers corresponding to the maximum and lower cut-off wavenumbers in the characteristic growth rate. We compare the theory to simulations of a nonequilibrium hybrid Ising/lattice-gas model exhibiting natural and forceful interconversion in addition to diffusion and obtain a qualitative agreement.

E-mail addresses: tlongo1@umd.edu (T.J. Longo), nshum@bu.edu (N.A. Shumovskyi), buldyrev@yu.edu (S.V. Buldryev), anisimov@umd.edu (M.A. Anisimov).

https://doi.org/10.1016/j.nocx.2022.100082

Received 30 September 2021; Received in revised form 31 December 2021; Accepted 9 January 2022 Available online 13 January 2022

<sup>\*</sup> Corresponding author.

#### 2. Modified Cahn-Hilliard-Cook theory

In this section, we generalize the Cahn-Hilliard theory of spinodal decomposition to allow for both natural and forceful interconversion of species and derive the structure factor for concentration fluctuations.

#### 2.1. Generalized spinodal decomposition

The effect of interconversion on the temporal evolution of the concentration for a symmetric binary mixture of species A and B in the presence of interconversion is given in the simplest form [16] as

$$\frac{\partial \widehat{c}_A}{\partial t} = M \nabla^2 \widehat{\mu} - L \widehat{\mu} - K \widehat{c}_A \tag{1}$$

where  $\widehat{c}_A$  is the order parameter, related to the physical concentration of species A by  $\widehat{c}_A=2c_A-1$ , M and L are kinetic coefficients for the mutual diffusion and natural (spontaneous) interconversion dynamics respectively, and the third term is an external source of forceful interconversion. We consider the case when interconversion, both natural and forceful, occurs through a reaction  $A \rightleftharpoons B$  where K is the forward and reverse reaction rate. Physically, a source of forceful interconversion could be introduced via irradiation through photons [21] which promote interconversion of species or it could be introduced through a flux of matter [22]. In the absence of interconversion, when L=0 and K=0, then Eq. (1) reduces to the Cahn-Hilliard theory [20]. Lastly, the reduced chemical potential difference,  $\widehat{\mu}=\widehat{\mu}_A-\widehat{\mu}_B$ , is found from the variational derivative of the dimensionless Landau-Ginzburg free-energy functional [16] as

$$\widehat{\mu} = \frac{\mu}{k_{\rm B} T_c} = \frac{1}{2} (1 + \Delta \widehat{T}) ln \left( \frac{1 + \widehat{c}_A}{1 - \widehat{c}_A} \right) - \widehat{c}_A - \kappa \nabla^2 \widehat{c}_A$$
 (2)

where the reduced distance to the critical temperature,  $\Delta \widehat{T} = 1 - T/T_c$ , is negative in the spinodal (unstable) region,  $k_B$  is Boltzmann's constant, and  $\kappa$  is the square of the range of intermolecular interactions. In this work, we adopt  $\kappa=1$  in the units of the square of the molecular size. Expanding Eq. (2) to first order and analytically evaluating Eq. (1) via a Fourier transform, the characteristic growth rate, known as the "amplification factor" [13,16,20], for spinodal decomposition in the presence of interconversion may be written in the form [16].

$$\omega(q,t) = M\kappa q_m^2(t) [q_m^2(t) - 2q_-^2] - M\kappa [q^2 - q_m^2(t)]^2$$
(3)

where the two characteristic wavenumbers,  $q_m$  and  $q_-$ , are the maximum and the lower cut-off of the amplification factor, respectively (see Fig. 1a). Using a first order approximation, they have the form

$$q_m^2 = -\frac{(\widehat{M}_{q=0}^{-1}(t) + L\kappa)}{2M\kappa} \quad \text{and}$$

$$q_-^2 = -\frac{(K + L\Delta \widehat{T})}{M\Delta \widehat{T} + L\kappa}$$
(4)

We note that the maximum of the amplification factor,  $q_m = q_m(t)$  is time dependent, while we hypothesize that  $q_-$  is time independent. The time dependence of  $q_m(t)$  is given through the higher order terms of the chemical potential, Eq. (2), and is introduced into the time-dependent inverse thermodynamic susceptibility,  $\widehat{\chi}_{q=0}^{-1}(t) = \partial \widehat{\mu}/\partial \widehat{c}_A(t)$ . The origin of this temporal evolution is due to the change in concentration at constant temperature from the unstable  $(\widehat{c}_A = 0)$  to the stable  $(\widehat{c}_A > 0)$  regime; as such, in the second order approximation,  $\widehat{\chi}_{q=0}^{-1}(t) \simeq \Delta \widehat{T} + (1 + \Delta \widehat{T})\widehat{c}_A^2(t)$  [16,23,24]. In contrast,  $q_-$  is an intrinsic property of the system, and since  $q_-$  determines the cut-off for the smallest possible growing domain modes, then the steady-state limit of the time evolution of the maximum wavenumber will also be cut-off by  $q_-$  as  $q_m(t \to \infty) \propto q_-$ . To verify this prediction, we numerically compute  $q_m$  from the wavenumber corresponding to the maximum of the structure factor,  $q_m$ , so

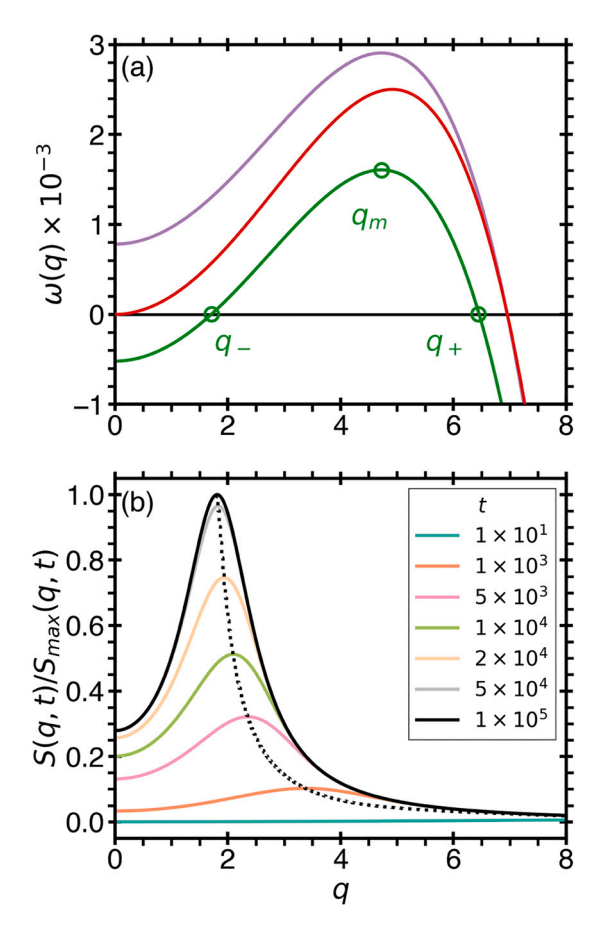


**Fig. 1.** a) The amplification factor,  $\omega(q)$ , given by Eq. (3), for  $\kappa = 1$  and  $\Delta \hat{T} = 0$ 0.1. The red curve represents the Cahn-Hilliard theory (phase separation) for M = 1, L = 0, and K = 0; the purple curve represents phase amplification for M= 1, L = 1/127, and K = 0; the green curve represents the generalized Cahn-Hilliard theory in the presence of natural and forceful interconversion for M= 1, L = 1/127, and  $K = 1.3 \times 10^{-3}$ . For the latter case (with forceful interconversion), the green circles indicate the three characteristic wavenumbers of the amplification factor: the maximum,  $q_m$ , the lower cut-off,  $q_-$ , and the upper cut-off,  $q_+$ . b) The time evolution of the structure factor, given by Eq. (9), for the same parameters used in the generalized Cahn-Hilliard-Cook theory in the presence of natural and forceful interconversion. The black dotted line depicts the evolution of the maximum of the structure factor. Due to the external source of forceful interconversion, the maximum of the structure factor is interrupted at the wavenumber  $q_{-}$ , while for complete phase separation and phase amplification, the maximum of the structure factor will evolve to q = 0 for an infinitesized system. (For interpretation of the references to colour in this figure legend, the reader is referred to the web version of this article.)

and compare our results with the steady-state domain modes obtained from simulations of a nonequilibrium hybrid model.

# 2.2. Structure factor modified by interconversion of species

Defining the order parameter fluctuation variable as  $\delta \widehat{c}(\mathbf{r},t)$ , the structure factor is given through the correlation function for the concentration fluctuations [25]; such that

$$S(q,t) = \int d\mathbf{r} < \delta \widehat{c}(\mathbf{r},t) \delta \widehat{c}(\mathbf{r}_0,t). > e^{i\mathbf{q}\cdot\mathbf{r}}$$
(5)

As shown by Cook [26] and Langer et al. [27], the equation of motion for S(q,t) is found by introducing order-parameter fluctuations into the time evolution of the order parameter, Eq. (1), with  $\delta\widehat{c}(\mathbf{r})$  as the fluctuation variable and spatially integrating  $\left\langle |\delta\widehat{c}|^2 \right\rangle$ . Following this procedure, we obtain the first-order solution for mixed diffusion-

interconversion dynamics as

$$\frac{\partial S(qt)}{\partial t} = 2\omega(qt)S(qt) + 2(Mq^2 + L\kappa)$$
 (6)

where  $\omega(q,t)$  is given by Eq. (3) [28–30]. We note that in the absence of interconversion and forceful racemization, this equation reduces to the result presented by Cook [26]. Solving this differential equation for the structure factor, assuming a linear approximation [23], with the condition  $\partial \omega/\partial t \ll \omega(q,t)$ , gives [24,31–33].

$$S(q,t) = S_{\infty}(q) + [S(q,t=0) - S_{\infty}(q)]e^{2\omega(q,t)t}$$
(7)

where S(q,t) represents the modified Cahn-Hilliard-Cook structure factor, which now includes natural and forceful interconversion. In the limit of infinite time, when  $\partial S(q,t)/\partial t=0$ , the steady-state structure factor,  $S_{\infty}(q)$ , is given by

$$S(q, t \to \infty) = S_{\infty}(q) = \frac{Mq^2 + L\kappa}{-\omega(q, t \to \infty)}$$
(8)

It can be seen that when either L=0 or M=0, then this equation, in equilibrium conditions (K=0), reduces to the Ornstein-Zernike structure factor -  $S_{OZ}=\xi^2/(1+\xi^2q^2)$ , where the correlation length of concentration fluctuations is  $\xi^2=-\kappa/\Delta \hat{T}$ .

The time-dependent structure factor, Eq. (7), can be simplified by applying the condition that at t=0, the system is quenched from a sufficiently high temperature where S(q,t=0)=0. Therefore, Eq. (7) may be written as

$$S(q,t) = S_{\infty}(q) \left(1 - e^{2\omega(q,t)t}\right) \tag{9}$$

which is valid from the initial stages of spinodal decomposition to the coarsening regime [32,34]. Evaluating  $\partial S_{\infty}/\partial q=0$  to determine the wavenumber corresponding to the maximum of the structure factor gives  $q_m^s=2^{1/4}q_-$  in the steady-state limit. The time evolution of the structure factor is illustrated in Fig. 1b. To account for the time dependence of  $q_m(t)$ , we assume a simple approximation of the transition in the form  $q_m(t)=q_m(t=0)$  exp  $(-t/\tau)+q_-(1-\exp(-t/\tau))$  based on the limiting values of  $q_m$  at t=0 and  $t\to\infty$ , where  $\tau$  is a system dependent parameter that controls the crossover from spinodal decomposition to the coarsening regime. As shown in Fig. 1, where we have selected  $\tau=100$ , the wavenumber corresponding to the maximum of the steady-state structure factor,  $q_m^s$ , aligns with the prediction of  $q_-$  from the theory. To accurately match the predictions from the theory with the computational results presented in the following section, we scale the characteristic wavenumbers from the theory by the size of the system.

#### 3. Methods

# 3.1. Spatial and temporal evolution of the order parameter

Using the finite difference method [35], with a spatial step  $\Delta x=1$  and a time step  $\Delta t=0.015$ , we calculate the temporal evolution of the order parameter given by Eq. (1) with a chemical potential given by Eq. (2). We observed that for time steps  $\Delta t>0.015$ , the solution diverges [35]. We include a random force term,  $\eta$ , to account for the thermal motion of the particles [26,32]. The system is initialized on an  $\ell \times \ell \times \ell$  cubic lattice with positions varied with initial random Gaussian noise,  $\sigma_i$ . The structure factor is calculated via a Fast Fourier Transform (FFT) of the order parameter throughout the system [35].

## 3.2. Nonequilibrium Ising/lattice-gas hybrid model

We consider an "Ising-like" lattice model where mutual diffusion is modeled by "swapping" the position of two neighboring species and interconversion is modeled by "flipping" one species type to another [13]. The diffusion and interconversion dynamics are simulated using a

hybrid of Kawasaki and Glauber Monte Carlo (MC) methods [25,36,37], respectively. The species are arranged on an  $\ell \times \ell \times \ell$  cubic lattice with a coordination number of 6. Using the Ising model Hamiltonian [38]

$$H = -\frac{\varepsilon}{2} \sum_{i=1}^{\ell^3} \sum_{j \in \Omega(i)} s_i s_j \tag{10}$$

where  $s_i$ ,  $s_j=\pm 1$  are spins,  $\Omega(i)$  is the set of 6 nearest neighbors of spin i, and  $\varepsilon$  is the interaction energy. The critical temperature of this system is  $T_c=4.5115(1)\varepsilon/k_B$  [39]. Realizations are initialized with a random spin configuration in which  $\ell^3/2$  spins are positive and the other  $\ell^3/2$  spins are negative. In addition, we assume that at each MC step the probability of a random spin flip (a Glauber step) is  $p_r$ , while the probability of swapping a randomly selected pair of nearest neighbor spins (a Kawasaki step) is  $1-p_r$ .

The equilibrium formulation, detailed in Ref. [13], is converted to nonequilibrium via the introduction of an additional energy, E, incorporated into the Boltzmann factor for the probability that a spin flip will be accepted as  $p \sim \exp \left[-(\Delta U - E)/k_{\rm B}T\right]$ , in which  $\Delta U$  is the difference in internal energy of the system for this step [40]. Thus, the effect of the energy source only affects the interconversion dynamics of the system. The diffusion dynamics, determined in each Kawasaki step, occur with a probability that two spins will swap according to the Metropolis criterion without any additional energy source. We introduce a sizeindependent MC time as  $t = n/\ell^3$ , such that in every time unit, each spin in the system has a chance,  $p_r$ , to flip, or a chance,  $1 - p_r$ , to swap with a neighboring spin. The probability of spin flipping is related to the diffusion and interconversion kinetic coefficients, M and L respectively, through  $p_r = L/(M+L)$  [13]. Additionally, the frequency of spin flipping is absorbed into the time step,  $\delta t$ , so that the kinetic coefficients, and consequently  $p_r$ , do not depend on temperature.

The dynamic structure factor is calculated using the method described in Kumar et al. [41]. This method differed from the FFT method, used in Section 3.2, since the maximum of the structure factor (after normalizing by  $\ell^3$ ) differed by a factor of  $\pi$ . Additionally, using the FFT method, the time evolution of the structure factor was interrupted at the wavenumber q=1 (indicating that the size of the two phase domains were half the size of the simulation box,  $\ell/2$ ), while using the method presented in Kumar et al., the maximum of the structure factor was interrupted at a larger wavenumber. To correct for this difference, we scale the wavenumbers such that complete phase separation occurs at q=1.

#### 4. Results and discussion

We confirmed that the presence of a source of forceful interconversion causes the system to phase separate into steady-state microphase domains as presented in Fig. 2(a-d). Due to the periodic boundary conditions imposed in the continuum finite-difference method used to compute Eq. (1), we found that the stripe morphologies will form at any angle with respect to the simulation box. The characteristic size of the stripe-like domains decreases with increasing forceful interconversion source strength, K. We note that a condition for microphase separation is that K must be sufficiently "strong" as to overcome the natural interconversion. If the magnitude of *K* is not strong enough, then (depending on the rate of natural interconversion) the system will either undergo phase amplification or complete phase separation. For instance, for M =1, L = 1/127,  $\Delta \hat{T} = -0.1$ , and  $K \le 4 \times 10^{-4}$ , then microphase separation is not observed. Since L = 1/127, the interconversion rate is relatively slow, and thus, the system has a higher probability of forming an interface between phases as shown in Fig. 2a. However, for a system with natural interconversion, this state is metastable, and eventually, the interface between phases will break down and phase amplification will occur [13].

The time-dependent structure factors, which produce the stripe-like

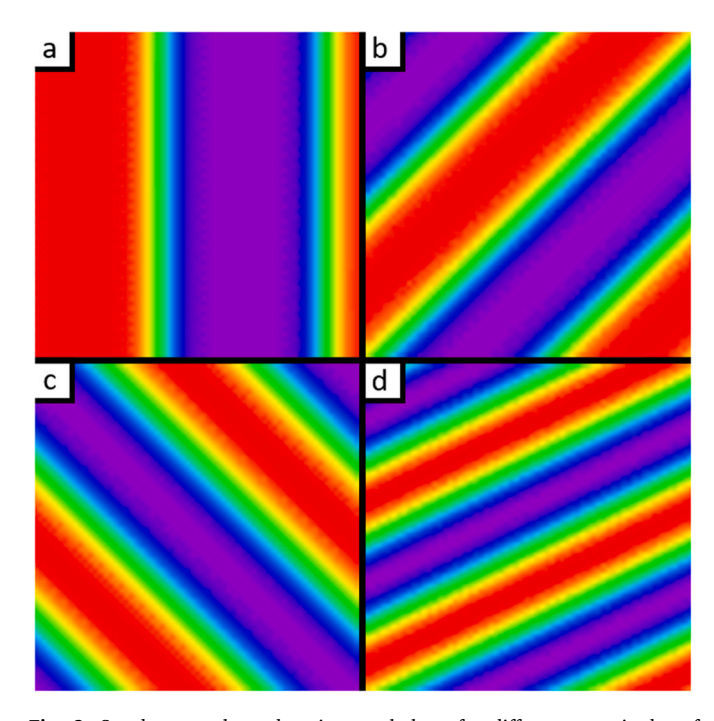


Fig. 2. Steady-state phase domain morphology for different magnitudes of forceful interconversion (after  $\sim \! 10^5$  time steps) computed from the time evolution of the order parameter, Eq. (1), with  $M=1, L=1/127, \Delta \widehat{T}=-0.1, \ell=64, \sigma_i=0.1, \eta=10^{-5}$ . Morphologies are shown for the middle slice of the three-dimensional system at (a) K=0, (b)  $K=5\times 10^{-4}$ , (c)  $K=15\times 10^{-4}$ , and (d)  $K=25\times 10^{-4}$ . The red regions correspond to where the value of the normalized order parameter is  $\widehat{c}_A/\widehat{c}_A^{\max}=1$ , the purple regions correspond to where the value of the normalized order parameter is  $\widehat{c}_A/\widehat{c}_A^{\min}=-1$ , and the other colors depict the interface between these two regions. The image in (a) depicts a metastable structure toward phase amplification [13], while the images in (b-d) are modulated steady-state structures with a characterize size,  $1/q_-$ . (For interpretation of the references to colour in this figure legend, the reader is referred to the web version of this article.)

morphology, as illustrated in Figs. 2(a-d), are presented in Figs. 3(a-d). We observe that the time evolution of the maximum of the structure factor in Fig. 3a is interrupted at the wavenumber q = 0, which corresponds to a system undergoing phase amplification. For  $K = 4 \times 10^{-4}$ (Fig. 3b), the maximum of the time evolution of the structure factor is interrupted at q = 1, indicating complete phase separation where the phase domains have a characteristic size of half the simulation box,  $\ell/2$ . In Fig. 3(c,d), the time evolution of the maximum of the structure factor is interrupted at higher wavenumbers depending on K. These wavenumbers correspond to the characteristic size of the stripe-like phase domains and are independent of the size of the system. We also observe that the structure factor at the maximum wavenumber  $(q_m)$  contains the largest uncertainty, with respect to the other wavenumbers. The nonmonotonic temporal evolution of the structure factor observed in Fig. 3b can be attributed to  $\tau \approx 1.5 \times 10^3$ , a large characteristic crossover time scale between spinodal decomposition and coarsening. This observation suggests that the crossover time scale,  $\tau = \tau(K)$ , may depend on forceful interconversion.

The temporal evolution of the order parameter was calculated from Eq. (1) using the chemical potential given in Eq. (2). The average value of the order parameter, calculated by first averaging over all space and second averaging the absolute value over N=100 realizations, is presented in Fig. 4a. This method of averaging highlights the behavioral deviation from  $\widehat{c}_A=0$ , when the concentration of species A is equivalent to species B; therefore, this figure represents the temporal evolution of the symmetry of phase separation. We observed that the initial value  $\langle |\widehat{c}_A| \rangle$  is determined by  $\sigma_i$ , the random initial configuration, whereas the steady-state behavior of  $\langle |\widehat{c}_A| \rangle$  is determined by  $\eta$ , the thermal noise to be included in Eq. (1). We find that  $\langle |\widehat{c}_A| \rangle$  develops a peak during the formation of the stripe-like patterns. As the phase domains coarsen, the averaged order parameter reaches a steady-state value,  $\langle |\widehat{c}_A(t \to \infty)| \rangle = c_0$  indicating the stable formation of the stripe-like domains.

In Fig. 4b, we show the temporal evolution of the standard deviation of the averaged order parameter, calculated by first determining the standard deviation over all space and second by averaging over N=100 realizations. We observed that the N-averaged standard deviation,  $\langle \sigma \rangle_N$ , was constant through the early stages of spinodal decomposition, but dramatically increased during the formation of the stripe-like patterns. We note that in the K=0 case due to phase amplification  $\langle \sigma \rangle_N$  rapidly

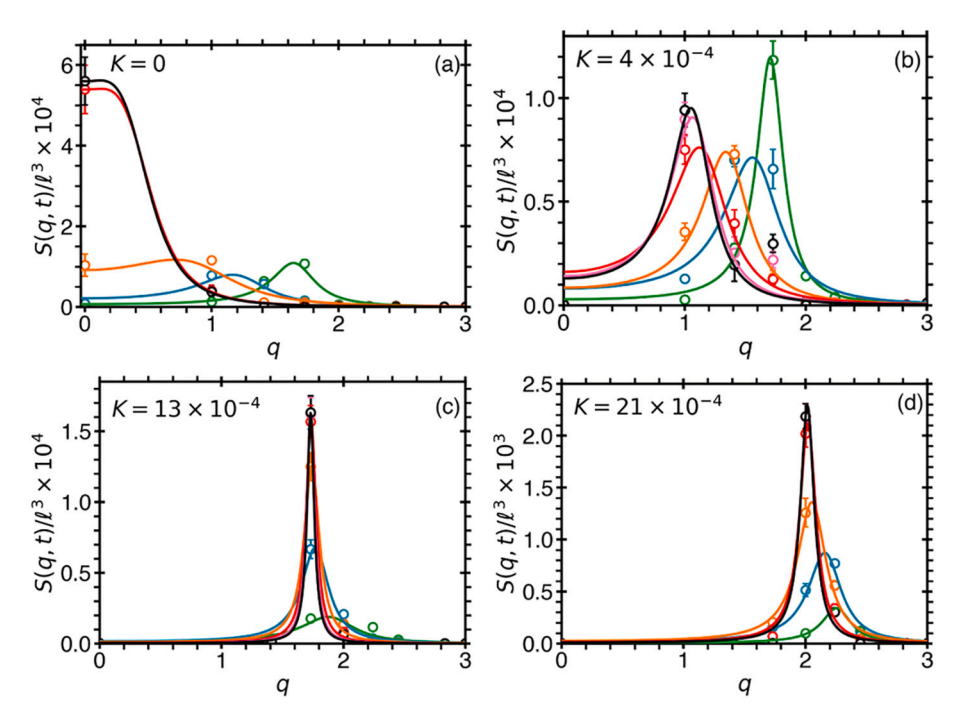
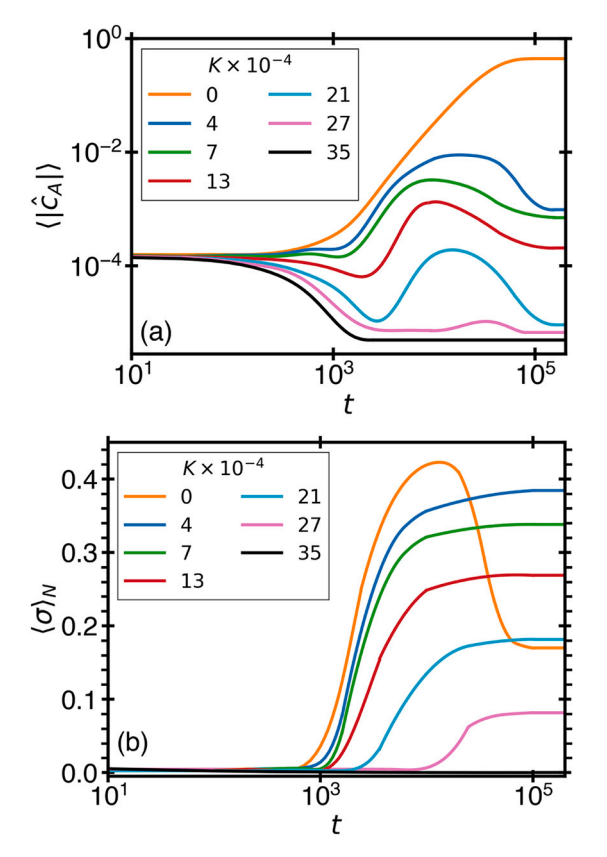


Fig. 3. Time evolution of the structure factor computed from the Fast Fourier transform (FFT) solution of Eq. (1) for  $M = 1, L = 1/127, \Delta \hat{T} = -0.1, \ell$ = 64,  $\sigma_i = 0.1$ ,  $\eta = 10^{-5}$  depicted at times  $t = 6 \times 10^3$ (green),  $t = 1.2 \times 10^4$  (blue),  $t = 2.4 \times 10^4$  (orange), t $= 5 \times 10^4$  (red),  $t = 1 \times 10^5$  (pink), and  $t = 2 \times 10^5$ (black). The open circles in (a-d) depict the computed structure factors for the four selected magnitudes of forceful interconversion averaged over N = 100 realizations with 95% confidence interval error bars, while the solid lines illustrate the behavior of the structure factors assuming a Gaussian distribution. In (a), the evolution of the maximum of the structure factor is interrupted at the wavenumber q = 0, corresponding to phase amplification, while in (b) the maximum is interrupted at q=1, corresponding to phase domains with a characteristic size of half the simulation box,  $\ell/2$ . In (c,d), the evolution of the maximum of the structure factor is interrupted at wavenumbers  $q = q_- > 1$  corresponding to microphase separation. (For interpretation of the references to colour in this figure legend, the reader is referred to the web version of this article.)



**Fig. 4.** The temporal evolution of the symmetry of phase separation. a) The time evolution of the average order parameter, calculated by first averaging over all space and second by averaging the absolute value over N=100 realizations, for  $M=1, L=1/127, \Delta T=-0.1, \sigma_i=0.1, \eta=1.0\times 10^{-5},$  and various magnitudes of forceful interconversion, K. b) The time evolution of the N-averaged standard deviation of the averaged order parameter, calculated by first determining the standard deviation of the spatially averaged order parameter and second by averaging over N=100 realizations. This method of averaging highlights the behavioral deviation from an equal concentration of species A and B,  $\hat{c}_A=0$ .

increases as the domains coarsen, but then decreases when one phase grows at the expense of the other. In this case, the constant steady-state limit of the averaged standard deviation,  $\langle \sigma(t \to \infty) \rangle_N = \sigma_0$ , indicates that the order parameter has reached its equilibrium value,  $|\hat{c}_A| = c_0$ , which depends on the distance to the critical temperature.

In Fig. 5(a,b), we compare the structure factor theory with simulations of the nonequilibrium hybrid model (defined in Section 3.2). In Fig. 5a, we show the steady-state structure factor from simulations at three different additional energy values, E, at constant temperature,  $\Delta \hat{T} = -0.4$ , averaged over N = 60 realizations. Unlike the morphologies computed from Eq. (1) via the finite-difference method, the snapshots of the MC simulations shown in the insets of Fig. 5a depict stripe-like phase domains that form along the diagonal of the simulation box. We attribute this affect to the lattice structure utilized in the MC simulations. We introduce three system-dependent constants into the steady-state structure factor (when  $q_m \sim q_-$ ) and use Eq. (8) in the form

$$S_{\infty}(q) = \frac{S_0 a^2 (q^2 + L_{\text{eff}})}{a^2 q_-^4 + \left[ q^2 - (1+a) q_-^2 \right]^2}$$
 (11)

where the amplitude ratio relating the theory to the nonequilibrium hybrid model is  $S_0=46.5$  and the effective interconversion kinetic coefficient is  $L_{\rm eff}\sim L/M=0.0012$ . The constant a=0.2, which describes the relationship between  $q_m(t\to\infty)$  and  $q_-$ , broadens or sharpens the scattering peak. At the maximum of the structure factor, when  $q=q_-$ ,

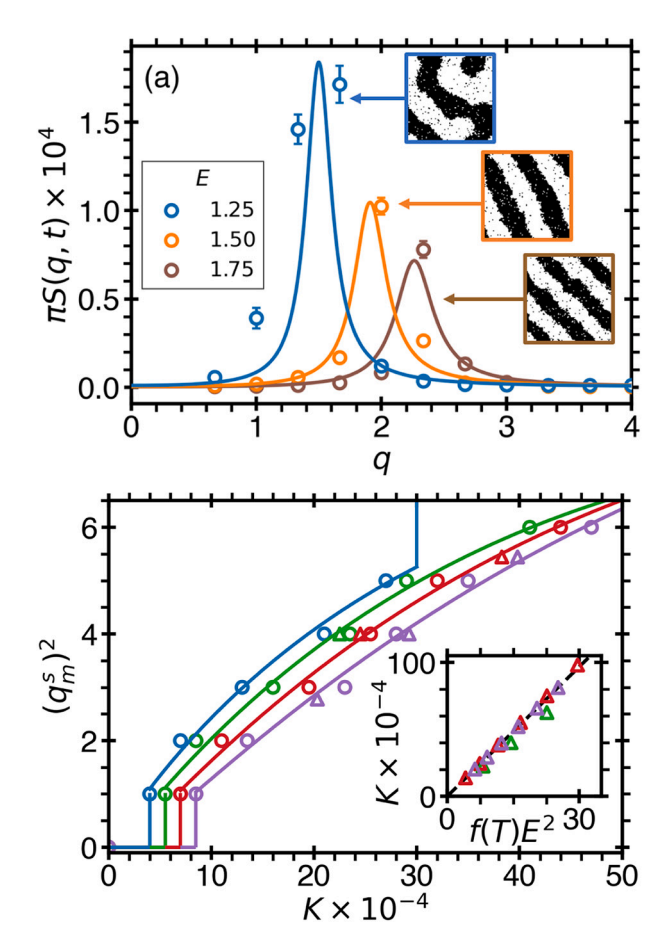


Fig. 5. a) Steady-state structure factors computed for the nonequilibrium hybrid model (open circles) and the prediction given by Eq. (11) (solid lines) for selected external energy sources (E) at  $\Delta \widehat{T} = -$  0.4, M = 1 , L = 1/127 ,  $\ell = 100$  . and averaged over N = 60 realizations with 95% confidence interval error bars. The insets show steady-state ( $t \sim 3 \times 10^5$ ) domain morphologies observed in the nonequilibrium hybrid model for the selected energies. b) The dependence of the wavenumber corresponding to the maximum of the structure factor,  $q_m^s$ , on the forceful interconversion source strength K, in the steady-state limit. The open circles are numerical computations of structure factors determined from FFTs of the time evolution of the order parameter, given by Eq. (1), in the steady-state limit ( $t \sim 10^5$ ) for M = 1, L = 1/127,  $\sigma_i = 0.1$ , and  $\eta = 10^{-5}$ , averaged over N = 100 realizations. The triangles correspond to the predictions of K determined from fits of Eq. (11) to the structure factor for the nonequilibrium hybrid model, like those presented in (a). The curves illustrate the theoretical prediction  $q_m(t \to \infty) \propto q_-$ , given by the full expression for  $q_-$ , found from evaluating  $\omega(q,0)=0$  using Eq. (3). The colors correspond to temperatures:  $\Delta \hat{T} = -0.1$  (blue),  $\Delta \hat{T} = -0.2$  (green),  $\Delta \hat{T} = -0.3$  (red), and  $\Delta \hat{T} = -0.4$ (purple). The inset shows the relationship between *K* and *E*. (For interpretation of the references to colour in this figure legend, the reader is referred to the web version of this article.)

then Eq. (11) reduces to  $S_{\infty}(q_{-}) = S_{0}/(2q_{-}^{2})$ , which is independent of a. We note that in this form, Eq. (11) resembles the scattering intensity distribution of microemulsions [42].

In Fig. 5b, the dependence of the wavenumber corresponding to the maximum of the structure factor,  $q_m^s$ , on the magnitude of forceful interconversion, K, is illustrated for the theoretical prediction (curves), computations of the time evolution of the order parameter (circles), and simulations of the nonequilibrium hybrid model (triangles). The curves are determined from the full expression for the lower cut-off wavenumber,  $q_-$ , found from Eq. (3), when  $\omega(q,0)=0$ . A variable amplitude and shift are introduced to scale the theoretical prediction of  $q_-$  such that microphase separation begins at q=1. An additional system dependent constant is introduced to describe the relationship between

 $q_m(t \to \infty)$  and  $q_-$ . The numerical computations of  $q_m{}^s$  (averaged over N=100 realizations) from the time evolution of the order parameter, Eq. (1), are shown in the steady-state regime (after  $t\sim 10^5$  time steps). The magnitude of forceful interconversion, K, (for different external energies, E) was obtained for the nonequilibrium hybrid model using Eq. (11). In the inset of Fig. 5b, we illustrate the relationship between theory and the nonequilibrium hybrid model, as  $K \propto E^2$ .

In addition, as illustrated by Fig. 5b, we find two values of forceful interconversion,  $K^*$  and  $K^{**}$  (indicated by the vertical lines), that bound the formation of microphase domains. Both boundaries increase with  $\Delta \hat{T}$ ; such that, for  $\Delta \hat{T} > -0.1$ ,  $K^{**}$  is located off the scale of the figure. For  $K < K^*$ , phase amplification was observed, while for  $K > K^{**}$ , no striped patterns were observed; instead, only a homogeneous solution persisted, in which an apparent structure on a small scale may be attributed to the correlations between concentration fluctuations. In this case, the particles are forced to interconvert so rapidly that diffusion is impossible. As shown in Fig. 5b, the lower bound,  $K^*$ , is associated with the characteristic wavenumber,  $q^* = q = 1$ , which corresponds to phase domains that form at half the size of the simulation box,  $\ell/2$ . In contrast, the characteristic wavenumber associated with the upper bound,  $q^{**}$ , is strongly dependent on temperature [15,16].

We note that for  $\Delta \widehat{T} = -0.1$ , no structured microphase separation was observed in the nonequilibrium hybrid model. We attribute the lack of structured domains to the increase in concentration fluctuations facilitated by the close proximity to the critical point. This effect was not observed in the time evolution of the order parameter, shown in Fig. 2 (a–d), as the mean-field theory described in Section 2. is only applicable sufficiently far away from the critical point.

Lastly, as shown in Section 2, the wavenumber corresponding to the maximum of the structure factor,  $q_m^s$ , scales linearly with the lower cutoff wavenumber,  $q_-$ . Consequently, we observe the scaling law that  $q_m^s \sim \sqrt{K} \propto \sqrt{f(T)} E$ , where the temperature dependent prefactor is  $f(T) \simeq 9.71 T/(T_c-T)$ . This result, which verifies our initial hypothesis, has also been confirmed in studies of a chiral model where the source of forceful interconversion is established internally via dissipative intermolecular forces [15]. Interestingly, previous studies of phase separating block copolymers in the presence of forceful interconversion found that  $q_m^s \sim K^{1/4}$  [19,28]. As these previous studies considered an n-component order parameter to describe the block copolymer system (whereas, in this work, we describe our binary mixture via a single-component order parameter), this implies that the effect of K on  $q_m^s$  is system dependent and could depend on the nature of the order parameter.

### 5. Conclusion

We have demonstrated that the presence of a source of forceful interconversion in a hybrid binary system that possess both diffusion and natural interconversion dynamics may produce microphase separation. We characterize the time evolution of the phase formation through two characteristic wavenumbers,  $q_m$  and  $q_-$ , which correspond to the maximum and lower cut-off wavenumbers of the amplification factor obtained from the generalized theory of spinodal decomposition. In the infinite time (steady-state) limit, we showed that  $q_m(t \to \infty) \propto q_- \propto K^{1/2}$ , where K is the rate of forceful interconversion. We compared the structure-factor theory with Monte Carlo simulations of a nonequilibrium hybrid model and demonstrated that the origin of microphase separation may be related to an external energy source, as  $E \propto K^{1/2}$ , which allows domain formation to be more energetically favorable.

Our symmetric binary-mixture model with molecular interconversion of species represents the simplest case of liquid polyamorphism with the possibility of a liquid-liquid transition in a single-component substance. Indeed, the interconversion of species allows the concentration to be a thermodynamically dependent property, equivalent to the reaction coordinate. Therefore, the system, in terms of its thermodynamic degrees of freedom, behaves like a single-component substance

[12]. Thus, in our simple system, as in the Ising model, the equilibrium value of the reaction coordinate is always 50% above the critical temperature and contains two equilibrium values, corresponding to the coexisting liquid phases, below the critical temperature. Another simple system exhibiting liquid polyamorphism is a mixture of interconverting enantiomers [15]. In this system, the equilibrium interconversion fraction does not depend on temperature and pressure, like in our model. In the future, our approach could be generalized to more complex systems exhibiting or suggesting liquid polyamorphism, such as supercooled water [3], where the fraction of interconversion of alternative molecular or supramolecular states is usually a function of temperature and pressure [12,16].

Another possible application of our approach could be glassy polyamorphism, a largely unexplored area. It is commonly believed that the hypothesized liquid polyamorphism in supercooled water, which is possibly caused by the interconversion of alternative supramolecular structures, is related to the experimentally established existence of two glassy waters, high-density glass and low-density glass [3,43–45]. In this respect, it would be interesting to consider effects of structural interconversion in glassy systems. In addition, forceful interconversion, as a result of an external source of energy, may generate nonequilibrium microphase separation in glasses, similar to that studied in this work. These structures could be similar to the nonequilibrium nano-scale phase separation formed by "frozen" spinodal decomposition, as observed in metallic glasses [46]. This is another unexplored area of research.

#### **Declaration of Competing Interest**

The authors declare that they have no known competing financial interests or personal relationships that could have appeared to influence the work reported in this paper.

#### Acknowledgements

We thank Betül Uralcan and Pablo Debenedetti for useful discussions. This work is a part of the research collaboration between the University of Maryland, Princeton University, Boston University, and Arizona State University supported by the National Science Foundation. The research at the University of Maryland was supported by NSF Award No. 1856479. The research at Boston University was supported by NSF Award No. 1856496. S.V.B. acknowledges the partial support of this research through the Dr. Bernard W. Gamson Computational Science Center at Yeshiva College. We dedicate this work to the late C. Austen Angell, our friend, collaborator, and invaluable mentor.

# References

- C. A. Angell, Two-state thermodynamics and transport properties for water as zeroth-order results of a "bond lattice" model, J. Phys. Chem. 75 (24). doi: https://doi.org/10.1021/i100693a010.
- [2] C.A. Angell, Amorphous water, Annu. Rev. Phys. Chem. 55 (1) (2004) 559–583, https://doi.org/10.1146/annurev.physchem.55.091602.094156.
- [3] P. Gallo, K. Amann-Winkel, C.A. Angell, M.A. Anisimov, F. Caupin, C. Chakravarty, E. Lascaris, T. Loerting, A.Z. Panagiotopoulos, J. Russo, J.A. Sellberg, H.E. Stanley, H. Tanaka, C. Vega, L. Xu, L.G.M. Pettersson, Water: a tale of two liquids, Chem. Rev. 116 (13) (2016) 7463–7500.
- [4] S. Sastry, C.A. Angell, Liquidliquid phase transition in supercooled silicon, Nat. Mater. 2 (2003) 739–743, https://doi.org/10.1038/nmat994.
- [5] L. Xu, S.V. Buldyrev, C.A. Angell, H.E. Stanley, Thermodynamics and dynamics of the two-scale spherically symmetric jagla ramp model of anomalous liquids, Phys. Rev. E 74 (2006) 031108, https://doi.org/10.1103/PhysRevE.74.031108. URL. htt ps://link.aps.org/doi/10.1103/PhysRevE.74.031108.
- [6] M.H. Bhat, V. Molinero, E. Soignard, V.C. Solomon, S. Sastry, J.L. Yarger, C. A. Angell, Vitrification of a monatomic metallic liquid, Nature 448 (2007) 787–790, https://doi.org/10.1038/nature06044.
- [7] L. Xu, S.V. Buldyrev, N. Giovambattista, C.A. Angell, H.E. Stanley, A monatomic system with a liquid-liquid critical point and two distinct glassy states, J. Chem. Phys. 130 (2009), 054505, https://doi.org/10.1063/1.3043665.

- [8] E. Lascaris, M. Hemmati, S.V. Buldyrev, H.E. Stanley, C.A. Angell, Search for a liquid-liquid critical point in models of silica, J. Chem. Phys. 140 (2014) 224502, https://doi.org/10.1063/1.4879057.
- [9] E. Lascaris, M. Hemmati, S.V. Buldyrev, H.E. Stanley, C.A. Angell, Diffusivity and short-time dynamics in two models of silica, J. Chem. Phys. 142 (2015) 104506, https://doi.org/10.1063/1.4913747.
- [10] P.H. Poole, T. Grande, C.A. Angell, P.F. McMillan, Polymorphic phase transitions in liquids and glasses, Science 275 (1997) 322–323, https://doi.org/10.1126/ science 275 5298 322
- [11] H. Tanaka, Liquidliquid transition and polyamorphism, J. Chem. Phys. 153 (2020) 130901. https://doi.org/10.1063/5.0021045.
- [12] M.A. Anisimov, M. Duska, F. Caupin, L.E. Amrhein, A. Rosenbaum, R.J. Sadus, Thermodynamics of fluid Polyamorphism, Phys. Rev. X 8 (1) (2018), 011004, https://doi.org/10.1103/PhysRevX.8.011004.
- [13] N.A. Shumovskyi, T.J. Longo, S.V. Buldyrev, M.A. Anisimov, Phase amplification in spinodal decomposition of immiscible fluids with interconversion of species, Phys. Rev. E 103 (2021), L060101, https://doi.org/10.1103/PhysRevE.103.L060101.
- [14] N.D. Petsev, F.H. Stillinger, P.G. Debenedetti, Effect of configuration-dependent multi-body forces on interconversion kinetics of a chiral tetramer model, J. Chem. Phys. 155 (2021) 084105, https://doi.org/10.1063/5.0060266.
- [15] B. Uralcan, T.J. Longo, M.A. Anisimov, F.H. Stillinger, P.G. Debenedetti, Interconversion-controlled liquid-liquid phase separation in a molecular chiral model, J. Chem. Phys. 155 (2021) 204502, https://doi.org/10.1063/5.0071988
- [16] T.J. Longo, M.A. Anisimov, Phase Transitions Affected by Molecular Interconversion, ArXivdoi:2102.11148v5, URL, https://arxiv.org/abs/2102.11148.
- [17] S.C. Glotzer, D. Stauffer, N. Jan, Monte Carlo simulations of phase separation in chemically reactive binary mixtures, Phys. Rev. Lett. 72 (26) (1994) 4109–4112, https://doi.org/10.1103/PhysRevLett.72.4109.
- [18] S.C. Glotzer, E.A. Di Marzio, M. Muthukumar, Reaction-controlled morphology of phase-separating mixtures, Phys. Rev. Lett. 74 (11) (1995) 2034–2037, https://doi. org/10.1103/PhysRevLett.74.2034.
- [19] J.J. Christensen, K. Elder, H.C. Fogedby, Phase segregation dynamics of a chemically reactive binary mixture, Phys. Rev. E 54 (1996) R2212–R2215, https:// doi.org/10.1103/PhysRevE.54.R2212. https://link.aps.org/doi/10.1103/Ph vsRevE.54.R2212.
- [20] J.W. Cahn, Phase separation by spinodal decomposition in isotropic systems, J. Chem. Phys. 42 (1) (1965) 93–99, https://doi.org/10.1063/1.1695731.
- [21] R.A. Enrique, P. Bellon, Compositional patterning in immiscible alloys driven by irradiation, Phys. Rev. B 63 (134111) (2001) 45–65, https://doi.org/10.1103/ PhysRevB 63 134111
- [22] J. Verdasca, P. Borckmans, G. Dewel, Chemically frozen phase separation in an adsorbed layer, Phys. Rev. E 52 (1995) R4616–R4619, https://doi.org/10.1103/ PhysRevE.52.R4616. https://link.aps. org/doi/10.1103/PhysRevE.52.R4616.
- [23] J. Langer, M. Bar-on, Theory of early-stage spinodal decomposition, Ann. Phys. 78 (2) (1973) 421–452, https://doi.org/10.1016/0003-4916(73)90266-2.
- [24] C. Billotet, K. Binder, Dynamic correlation of fluctuations during spinodal decomposition, Phys. A: Stat. Mech. Appl. 103 (1) (1980) 99–118, https://doi.org/ 10.1016/0378-4371(80)90209-5.
- [25] A.J. Bray, Theory of phase-ordering kinetics, Adv. Phys. 51 (2) (2002) 481–587, https://doi.org/10.1080/00018730110117433.
- [26] H.E. Cook, Brownian motion in spinodal decomposition, Acta Metall. 18 (3) (1970) 297–306, https://doi.org/10.1016/0001-6160(70)90144-6.
- [27] J.S. Langer, M. Bar-on, H.D. Miller, New computational method in the theory of spinodal decomposition, Phys. Rev. A 11 (4) (1975) 1417–1429, https://doi.org/ 10.1103/PhysRevA.11.1417.

- [28] S.C. Glotzer, A. Coniglio, Self-consistent solution of phase separation with competing interactions, Phys. Rev. E 50 (1994) 4241–4244, https://doi.org/ 10.1103/PhysRevE.50.4241. https://link.aps.org/doi/10.1103/PhysRevE.50.4241
- [29] A. Coniglio, M. Zannetti, Multiscaling in growth kinetics, Europhys. Lett. (EPL) 10 (6) (1989) 575–580, https://doi.org/10.1209/0295-5075/10/6/012.
- [30] A. Coniglio, M. Zannetti, Novel dynamical scaling in kinetic growth phenomena, Phys. A: Stat. Mech. Appl. 163 (1) (1990) 325–333, https://doi.org/10.1016/0378-4371(90)90341-0. https://www.sciencedirect. com/science/article/pii/0378437190903410.
- [31] K. Binder, C. Billotet, P. Mirold, On the theory of spinodal decomposition in solid and liquid binary mixtures, Zeitschrift f
  ür Physik B Condensed Matter 30 (2) (1978) 183–195.
- [32] K. Binder, Collective diffusion, nucleation, and spinodal decomposition in polymer mixtures, J. Chem. Phys. 79 (1983) 6387, https://doi.org/10.1063/1.445747.
- [33] G.R. Strobl, Structure evolution during spinodal decomposition of polymer blends, Macromol. 18 (1985) 559–563.
- [34] J.W. Cahn, The later stages of spinodal decomposition and the beginnings of particle coarsening, Acta Metall. 14 (1966) 1685–1962.
- [35] W.H. Press, S.A. Teukolsky, W.T. Vetterling, B.P. Flannery, Numerical Recipes: The Art of Scientific Computing, 3rd edition, Cambridge Univesity Press, Cambridge, United Kingdom, 2007.
- [36] K. Kawasaki, Diffusion constants near the critical point for time-dependent Ising models, I, Phys. Rev. 145 (1) (1966) 224–230, https://doi.org/10.1103/ PhysRev.145.224. https://link.aps.org/doi/10.1103/PhysRev.145.224.
- [37] R.J. Glauber, TimeDependent statistics of the Ising model, J. Math. Phys. 4 (2) (1963) 294–307, https://doi.org/10.1063/1.1703954. http://aip.scitation.org/doi/abs/10.1063/1.1703954.
- [38] K. Huang, Statistical Mechanics, 2nd edition, John Wiley and Sons, Inc., 1987.
- [39] H.-O. Heuer, Critical crossover phenomena in disordered ising systems, J. Phys. A Math. Gen. 26 (6) (1993) L333–L339, https://doi.org/10.1088/0305-4470/26/6/ 007
- [40] N. Metropolis, R.L. Ashenhurst, Basic operations in an unnormalized arithmetic system, IEEE Trans. Elect. Comp. EC-12 (6) (1963) 896–904, https://doi.org/ 10.1109/PGEC.1963.263593.
- [41] P. Kumar, S.V. Buldyrev, F. Sciortino, E. Zaccarelli, H.E. Stanley, Static and dynamic anomalies in a repulsive spherical ramp liquid: theory and simulation, Phys. Rev. E 72 (2005) 021501, https://doi.org/10.1103/PhysRevE.72.021501. https://link.aps.org/doi/10.1103/PhysRevE.72.021501.
- [42] M. Teubner, R. Strey, Origin of the scattering peak in microemulsions, J. Chem. Phys. 87 (1987) 3195, https://doi.org/10.1063/1.453006.
- [43] N. Giovambattista, T. Loerting, B.R. Lukanov, F.W. Starr, Interplay of the glass transition and the liquid-liquid phase transition in water, Sci. Rep. 2 (2012) 390, https://doi.org/10.1038/srep00390.
- [44] K. Amann-Winkel, C. Gainaru, P.H. Handle, M. Seidl, H. Nelson, R. Bhmer, T. Loerting, Waters second glass transition, PNAS 110 (44) (2013) 17720–17725, https://doi.org/10.1073/pnas.1311718110.
- [45] T. Loerting, V. Fuentes-Landete, P.H. Handle, M. Seidl, K. Amann-Winkel, C. Gainaru, R. Bhmer, The glass transition in high-density amorphous ice, J. Non-Cryst. Solids 407 (2015) 423–430, https://doi.org/10.1016/j. jnoncrysol.2014.09.003.
- [46] D. Kim, W. Kim, E. Park, N. Mattern, J. Eckert, Phase separation in metallic glasses, Prog. Mater. Sci. 58 (8) (2013) 1103–1172, https://doi.org/10.1016/j. pmatsci.2013.04.002.